Earth Planet. Sci. Lett. 672 (2025) 119694

Contents lists available at ScienceDirect

Earth and Planetary Science Letters

journal homepage: www.elsevier.com/locate/epsl

Fading of a sulfate-methane transition in deep and hot subseafloor sediments from the Nankai Trough

Male Köster [a,b,*], Bo Liu [a], Akira Ijiri [c,d], Arthur J. Spivack [e], Yuki Morono [c], Fumio Inagaki [f,g], Verena B. Heuer [h], Sabine Kasten [a,b,h], Susann Henkel [a,h]

[a] Alfred Wegener Institute Helmholtz Centre for Polar and Marine Research, 27570 Bremerhaven, Germany
[b] Faculty of Geosciences, University of Bremen, 28359 Bremen, Germany
[c] Kochi Institute for Core Sample Research, Japan Agency for Marine-Earth Sciences and Technology, 783-8502 Nankoku, Japan
[d] Kobe University, Graduate School of Maritime Sciences, 658-0022 Kobe, Japan
[e] University of Rhode Island, Graduate School of Oceanography, RI, USA
[f] Advanced Institute for Marine Ecosystem Change (WPI-AIMEC), Japan Agency for Marine-Earth Sciences and Technology, 236-0001 Yokohama, Japan
[g] Department of Earth Sciences, Graduate School of Science, Tohoku University, 980-8578 Sendai, Japan
[h] MARUM - Center for Marine Environmental Sciences, University of Bremen, 28359 Bremen, Germany

ARTICLE INFO

Edited by: Dr H Bao

Keywords:
Deep biosphere
IODP site C0023
Temperature limit
Reactive transport modeling
Inverse SMT

ABSTRACT

Biogeochemical processes in subseafloor sediments change significantly over geological timescales due to changing oceanographic, climatic or depositional conditions. Using dynamic reactive transport modeling, we reconstructed the evolution of biogeochemical processes over the past 5.5 million years in ~1.2-km deep and up to 120 °C hot sediments from International Ocean Discovery Program Site C0023 in the Nankai Trough, which records a complex depositional and thermal history. A distinctive feature is an inverse sulfate-methane transition (SMT) with a broad overlap zone between sulfate and methane of ~100 m, located in 80° to 85 °C hot sediments. This temperature coincides with the known temperature limit of anaerobic methane-oxidizing microbial communities. Based on a reactive transport model, we show that the inverse SMT was established ~2.5 million years ago (Ma) after the onset of biogenic methanogenesis and anaerobic oxidation of methane (AOM) as a consequence of increased organic carbon burial. Depth-integrated AOM rates decreased markedly since the beginning of trench-style deposition and an associated rapid heating of ~50 °C across the sediment column ~0.4 Ma. We argue that the activity of anaerobic methane-oxidizing communities at the inverse SMT has already started to cease and that the SMT is in the process of disappearing. This is the first study that documents the successive fading of an SMT and the decrease in the efficiency of this microbial methane sink as a result of sediment temperature increasing beyond the threshold of being suitable for anaerobic methane-oxidizing microbial communities.

1. Introduction

The deep subseafloor biosphere is generally referred to sediments deeper than 5 m below seafloor (mbsf) and represents the largest organic carbon (C_{org}) reservoir on Earth (e.g., Horsfield et al., 2006). Organic matter degradation drives microbial activity in up to at least 2.5 km deep subseafloor sediments (Inagaki et al., 2015) and due to its vast extension, the deep subseafloor biosphere plays an important role in global biogeochemical cycles (D'Hondt et al., 2002, 2004; Inagaki et al., 2006; Hoshino et al., 2020). However, the microorganisms within subseafloor sediments are not only exposed to extreme energy-limited and nutrient-poor conditions, but they also face increasing temperatures with progressive burial, with a typical gradient of 30 °C per km (Inagaki et al., 2015; Lever et al., 2015). In laboratory experiments, microbial life has been shown to withstand 120 °C (e.g., Blöchl et al., 1997; Takai et al., 2008), but the upper temperature limit of the deep biosphere, and thus its lower boundary, is still unknown.

To explore the temperature limit of the deep biosphere and the prerequisite of microbial life under extreme conditions and nutrient limitation, International Ocean Discovery Program (IODP) Expedition 370 drilled Site C0023 down to 1180 mbsf in the Nankai Trough off Cape Muroto, Japan (Fig. 1; Heuer et al., 2017). Although the temperature

* Corresponding author.
E-mail address: male.koester@awi.de (M. Köster).

https://doi.org/10.1016/j.epsl.2025.119694
Received 1 April 2025; Received in revised form 10 October 2025; Accepted 15 October 2025
Available online 10 November 2025

increases from ~2 °C at the sediment-water interface up to 120 °$C \pm 3$ °C at the basement, vegetative cells and microbial activity were observed throughout the entire sediment column (Heuer et al., 2020; Beulig et al., 2022). However, cell concentrations and potential metabolic rates determined by radiotracer incubation experiments significantly dropped by two to three orders of magnitude above 45 °C, marking the temperature limit for the growth of mesophilic microorganisms (Heuer et al., 2020; Beulig et al., 2022). Besides a conventional sulfate-methane transition (SMT) located in the upper 5 m of the sediments (Shipboard Scientific Party, 2001), the present-day profiles of sulfate (SO_4^{2-}) and methane (CH_4) also display an inverse SMT at ~730 mbsf with elevated CH_4 concentrations above and increasing SO_4^{2-} concentrations below (Fig. 2A; Heuer et al., 2017). In contrast to a conventional SMT, where SO_4^{2-} diffusing from the overlying seawater into the sediment is consumed, SO_4^{2-} originating from greater depths is reduced at an inverse SMT. The formation of an inverse SMT has earlier been described in subseafloor sediments from the Peruvian shelf (Ocean Drilling Program (ODP) Sites 1226 and 1229; Contreras et al., 2013; Tsang and Wortmann, 2022), the Bering Sea (IODP Site U1341; Wehrmann et al., 2013) and the Gulf of Alaska (IODP Site U1417; Zindorf et al., 2019). The deep sulfate pool is often associated with sulfate supply from lateral inflow of seawater (e.g., Wehrmann et al., 2013) or from a basement aquifer (e.g., D'Hondt et al., 2004; Torres et al., 2015; Zindorf et al., 2019; Tsang and Wortmann, 2022). However, at Site C0023, the elevated SO_4^{2-} concentrations below 730 mbsf are likely the result of a relict SO_4^{2-} pool that was not consumed in the past (Köster et al., 2021).

Biogeochemical processes can change significantly on glacial-interglacial and longer geological timescales due to changing oceanographic, climatic and depositional conditions, thereby inducing typical non-steady state diagenesis in the sediment/pore-water system (e.g., Thomson et al., 1984; Kasten et al., 1998; Riedinger et al., 2005; Arndt et al., 2006; Henkel et al., 2012). For example, the SMT in subseafloor

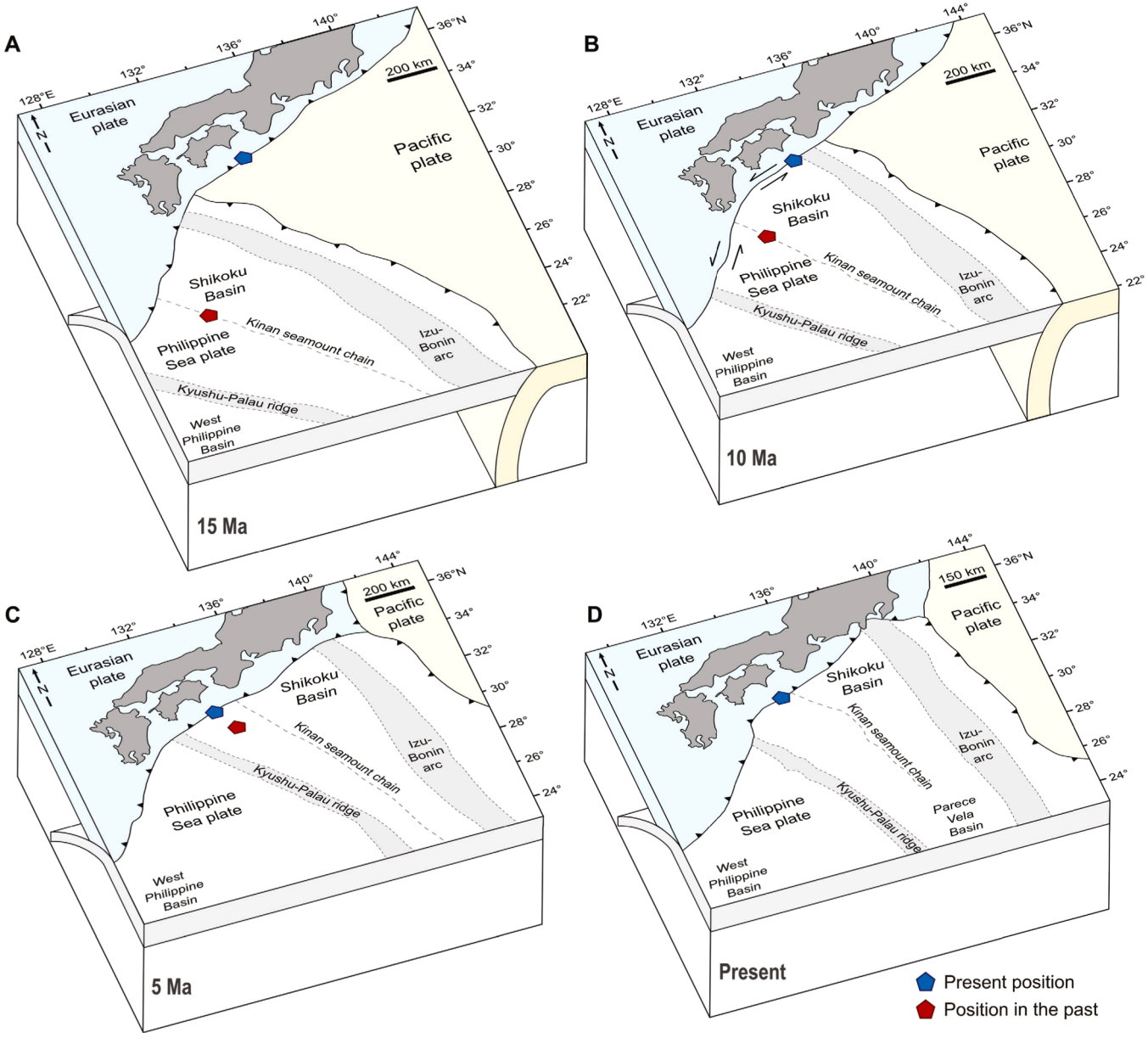

Fig. 1. Simplified schematic plate tectonic configuration of the Nankai Trough subduction zone offshore Japan in the northwestern Pacific Ocean and the relative movement of Site C0023 during its tectonically induced migration over the past 15 million years. Japan is held fixed at its current position. Blue and red symbols represent the present position of Site C0023 and its former position during the tectonic migration, respectively. Modified after Heuer et al. (2017), Lin et al. (2016) and Underwood and Guo (2018).

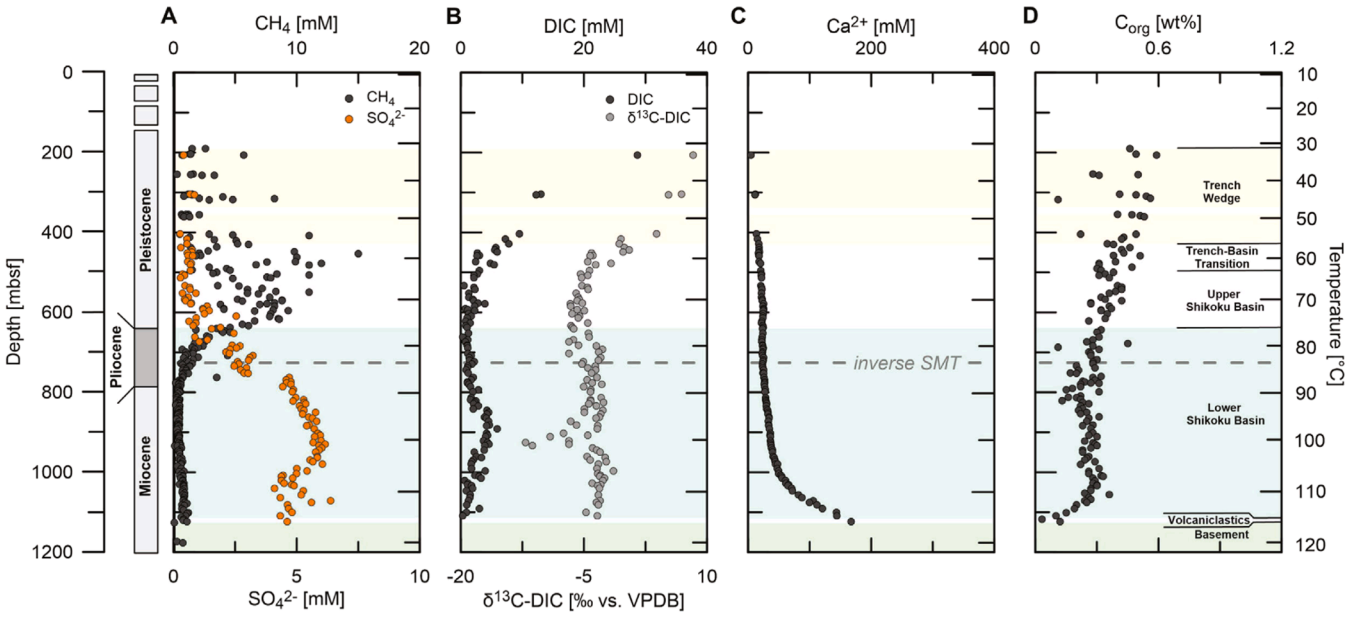

Fig. 2. Geochemical profiles of IODP Site C0023. Pore-water profiles of (A) sulfate (SO_4^{2-}) and methane (CH_4), (B) dissolved inorganic carbon (DIC) and its isotopic composition (δ^{13}C-DIC), (C) dissolved calcium (Ca^{2+}) and (D) solid-phase profile of organic carbon (C_{org}). All geochemical data except for δ^{13}C-DIC (this study), lithological units and temperature data are from Heuer et al. (2017) and (2020).

sediments from the Peruvian shelf has shifted in response to cyclic changes in organic carbon flux over glacial-interglacial timescales (Contreras et al., 2013). Similarly, Wehrmann et al. (2013) have shown variations in the flux of CH_4 and SO_4^{2-} in sediments from the Bering Sea due to changes in the amount and quality of organic matter over the last 4.3 million years. While several studies have focused on the microbial distribution, diversity and metabolic activity in different subseafloor regions (e.g., D'Hondt et al., 2004; Kallmeyer et al., 2012), the evolution of microbial activity as a consequence of changing environmental conditions on longer timescales is less understood.

We have previously reconstructed the evolution of biogeochemical processes at Site C0023 over the past 15 million years along its tectonically induced migration of 750 km from the Shikoku Basin to the Nankai Trough (Fig. 1) and presented a conceptual geochemical process model (Köster et al., 2021). We demonstrated that significant changes in sedimentation rates, organic matter contents and thermal conditions led to a transition from an organic carbon-starved environment with predominantly aerobic respiration processes and deep sulfate penetration and preservation to elevated carbon burial and the onset of anaerobic electron-accepting processes including biogenic CH_4 production and anaerobic oxidation of methane (AOM).

Here, we assess the plausibility of the conceptual model by using reactive transport modeling. We simulate the SO_4^{2-} and CH_4 profiles including the depth of the SMT as a function of sedimentation rate, C_{org} burial and temperature. We further derive metabolic rates from the model and investigate how microbial activity within the deep SMT responded to burial and heating.

2. Material and methods

2.1. Geological and sedimentary setting

IODP Site C0023 (32°22.00N, 134°57.98E; 4776 m water depth) is situated SW of Japan in the Nankai Trough, where the Philippine Sea plate is subducting beneath the Eurasian plate (Fig. 1; Heuer et al., 2017). The Nankai Trough is characterized by anomalously high heat flows (Yamano et al., 1992). With a geothermal gradient of 110 °C km^{-1}, the temperature at Site C0023 increases from ~2 °C at the sediment-water interface up to 120 °C ± 3 °C in the deepest core retrieved from the basement at 1177 mbsf (Heuer et al., 2020).

The ~1.2 km-thick sediment sequence at Site C0023 can be classified into five lithological units (Table 1). The volcaniclastic facies is the oldest unit that accumulated on the ~16 million-year-old basaltic basement when Site C0023 was located close to the spreading center of the Shikoku Basin (Fig. 1A). It is overlain by the Lower and Upper Shikoku Basin facies, both characterized by hemipelagic bioturbated mudstones (Taira et al., 1992). Site C0023 has moved ~750 km relative to its present geographic position from the central Shikoku Basin to the Nankai Trough due to tectonic motion of the Philippine Sea plate (Fig. 1; e.g., Mahony et al., 2011). The Trench-Basin Transition and the Trench Wedge facies (Unit IIA and IIB) accumulated on the ~600 m thick sequence of basin-style deposited hemipelagic mudstones when Site C0023 reached the subduction zone (Fig. 1D). The trench facies are characterized by turbidite-deposited mud, silt and sand (Taira et al., 1992). The transition from basin- to trench-style deposition led to a significant increase in sedimentation rates by two orders of magnitude from ~5.0 during deposition of the Lower Shikoku Basin facies to ~130 cm kyr^{-1} during deposition of the Trench Wedge facies (Table 1; Hagino and the Expedition 370 Scientists, 2018). This increase in sedimentation rates was accompanied by a rapid temperature increase of about 50 °C across the entire sediment column (Horsfield et al., 2006; Heuer et al., 2020; Tsang et al., 2020). At present, the C_{org} contents are overall low (<0.6 wt %; Fig. 2D; Heuer et al., 2017). The deep inverse SMT, where downward diffusing CH_4 intersects with upward diffusing SO_4^{2-}, which is preserved in the Lower Shikoku Basin facies, is located at ~730 mbsf (Fig. 2A; Heuer et al., 2020; Köster et al., 2021), with CH_4 and SO_4^{2-} overlapping in a relatively broad zone of ~100 m (Fig. 2A).

2.2. Geochemical analyses

In this study, we use sulfate (SO_4^{2-}), dissolved inorganic carbon (DIC), methane (CH_4), calcium (Ca^{2+}) and total organic carbon (C_{org}) data from Site C0023 obtained during IODP Expedition 370 (Heuer et al., 2017). All pore-water, gas and sediment measurements were performed onboard *D/V Chikyu* according to IODP standard protocols (Morono et al., 2017).

The carbon isotopic composition of DIC (δ^{13}C-DIC) was determined via isotopic ratio monitoring-gas chromatography mass spectrometry

Table 1
Lithological units and associated facies, lithology, depth range, age and sedimentation rates at IODP Site C0023 (Heuer et al., 2017). Ages and sedimentation rates are based on biostratigraphy studies of calcareous nannofossil assemblages (Hagino and the Expedition 370 Scientists, 2018).

Unit	Facies	Lithology	Depth [mbsf]	Age [Ma]	Sedimentation rate [cm kyr^{-1}]
IIA	Axial Trench Wedge	Hemipelagic and pelagic sand, muddy sand, turbidite-deposited silt and sandstones	189–318.5		
IIB	Outer Trench Wedge	Hemipelagic and pelagic mud, turbidite-deposited mudstones	353–428	0.29	131.9
IIC	Trench-Basin Transition	Turbidite-deposited silt and sand, tuffs and volcaniclastic sediments	428–494	0.29–0.43	61.0
III	Upper Shikoku Basin	Heavily bioturbated volcaniclastic mudstones	494–637.5	0.43–2.53	9.3–6.0
IV	Lower Shikoku Basin	Heavily bioturbated mudstones with green ash-rich laminae	637.5–1112	2.53–13.53	6.0–3.5
V	Acidic volcaniclastics	Mudstones and felsic ash	1112–1125.9		
	Basaltic basement	Hyaloclastites	1125.9		

(GC-C-MS; Thermo Finnigan Delta Plus XP isotope-ratio mass spectrometer (IRMS) connected to TRACE GC Ultra gas chromatograph) (Ijiri et al., 2012) at the Kochi Institute for Core Sample Research, JAMSTEC, Japan. The δ^{13}C-DIC values are expressed relative to VPDB (Vienna Pee Dee Belemnite). The standard deviation from repeated carbon isotope analysis of the laboratory standard ($NaHCO_3$ solution) was <0.2‰.

2.3. Reactive transport modeling setup and parametrization

A one-dimensional reactive transport model (e.g., Berner, 1980; Boudreau, 1997) was used to simulate the past evolution of the SO_4^{2-} and CH_4 profiles. The reactive transport model consists of three dissolved species (SO_4^{2-}, CH_4 and DIC), one solid species (C_{org}) as well as three reactions (organoclastic sulfate reduction (SR), biogenic methanogenesis (MG), and anaerobic oxidation of methane (AOM)) and uses the one-dimensional (depth, z) advection-diffusion-reaction equations (Mogollón et al., 2016; Volz et al., 2020) for dissolved (Eq. (1)) and solid species (Eq. (2)):

$$\varphi_i \frac{\partial C_{i,j}}{\partial t} = \frac{\partial}{\partial z}\left(\frac{\varphi_i D_{i,j}}{\theta^2}\frac{\partial C_{i,j}}{\partial z}\right) - \frac{\partial \varphi_i v_i C_{i,j}}{\partial z} + \varphi_i \sum R_{i,j} \tag{1}$$

$$(1-\varphi_i)\frac{\partial G_{i,j}}{\partial t} = -\frac{\partial (1-\varphi_i) w_i G_{i,j}}{\partial z} + (1-\varphi_i)\sum R_{i,j} \tag{2}$$

where t is time, z is sediment the depth in meter below seafloor (mbsf) and i,j represent subscripts depicting depth and species-dependence, respectively; φ is the porosity (Eq. S1); C,G are the species concentration (dissolved (SO_4^{2-}, CH_4, DIC) and solid (C_{org}) species, respectively); D is the tortuosity-corrected diffusion coefficient (θ^2), which was calculated according to Boudreau (1996) as $\theta^2 = 1 - 2\ln(\varphi)$; v and w are the burial velocity of the dissolved (Eq. (S2)) and the solid phase (Eq. (S3)), respectively; $\Sigma R_{i,j}$ is the sum of the reactions affecting the given species j. The effects of bioturbation and bioirrigation are not considered in the model since biologically induced mixing affects the upper 10 cm of sediment, which is not the focus of this study.

The primary redox reactions include organoclastic sulfate reduction (SR; Eq. (3)), methanogenesis (MG; Eq. (4)), AOM (Eq. (5)) and the precipitation of gypsum and/or anhydrite ($CaSO_4{\cdot}nH_2O$; Eq. (6)):

$$2CH_2O + SO_4^{2-} \rightarrow 2HCO_3^- + H_2S \tag{3}$$

$$2CH_2O + H_2O \rightarrow HCO_3^- + CH_4 + H^+ \tag{4}$$

$$SO_4^{2-} + CH_4 + H^+ \rightarrow HCO_3^- + H_2S + H_2O \tag{5}$$

$$SO_4^{2-} + Ca^{2+} + nH_2O \rightarrow CaSO_4{\cdot}nH_2O \tag{6}$$

The rate of organic matter degradation (R_{TOC}) was modeled using a 3-G model in which the heterogeneity of organic matter and its evolution during burial is considered (Jørgensen, 1978). In the 3-G model, the organic matter pool is classified into three discrete fractions (labile C^1_{org}, metabolizable C^2_{org} and refractory C^3_{org}), whereby each fraction is characterized by a specific degradability. Following this assumption, the rate of organic matter degradation was calculated as follows:

$$R_{TOC} = -\sum_{i=1}^{3} \sigma_i C^i_{org} \tag{7}$$

where C^i_{org} and σ_i are the concentrations of organic carbon and the specific first-order degradability of each fraction, respectively (Jørgensen, 1978).

The rate expressions for SR (R_1), MG (R_2), AOM (R_3) and the precipitation of anhydrite and/or gypsum (R_4) are given by:

$$R_1 = R_{TOC}(1 - f_s) \tag{8}$$

$$R_2 = R_{TOC} f_s \tag{9}$$

$$R_3 = k_{AOM} \times \frac{C_{CH4} C_{SO4}}{C_{SO4} + k_{s,AOM}} \tag{10}$$

$$R_4 = k_{pp} \times \left(\frac{C_{Ca} C_{SO4}}{K_{sp}} - 1\right). \tag{11}$$

The factor f_s (Eqs. (8) and (9)) is a rate-limiting term that determines the extent to which organoclastic sulfate reduction and methanogenesis are inhibited by sulfate. It is based on the complementary error function (erfc) defined by:

$$f_s = 0.5 \times erfc\left(\left(C_{SO4} - C^*_{SO4}\right) / k_{in}\right), \text{ where } f_s \sim \begin{cases} 1 \text{ if } C_{SO4} < C^*_{SO4} \\ 0 \text{ if } C_{SO4} > C^*_{SO4} \end{cases} \tag{12}$$

The terms C^*_{SO4} and k_{in} are the threshold sulfate concentration for methanogenesis and a parameter controlling steepness, respectively (Burdige et al., 2016a, 2016b). The AOM rate depends on a Monod type kinetic function with an inhibition constant $k_{S,AOM}$ of 1 mM (Nauhaus et al., 1995) and the rate constant k_{AOM} (Arndt et al., 2006). The factor k_{pp} is the kinetic rate constant of the $CaSO_4{\cdot}nH_2O$ precipitation and K_{sp} is the solubility product.

The temperature dependent rate constants k_{AOM} and $\sigma_{i=1-3}$ are defined as:

$$k_{AOM} = k^0_{AOM} f(T) F_{in}(T), \tag{13}$$

and

$$\sigma_{i=1-3} = \sigma^0_{i=1-3} f(T) F_{in}(T), \tag{14}$$

where k^0_{AOM} and σ^0_i are the AOM rate and organic matter degradation rate constants at the reference temperature, T_0, respectively; $f(T)$ determines the temperature dependency of the rate constant and $F_{in}(T)$ is a temperature-limiting term (LaRowe et al., 2014).

The temperature dependence of rate constants $f(T)$ is calculated using the temperature coefficient for reactions rates Q_{10} (LaRowe et al., 2014):

$$f(T) = Q_{10}^{\frac{T-T_0}{10}}. \quad (15)$$

The value of Q_{10} indicates the factor by which the rate constants increase for every 10-degree increase in temperature compared to the reference temperature T_0 at the sediment surface (10 °C).

The temperature limiting term $F_{in}(T)$, which is based on the assumption that microbes grow or catalyse reactions over a finite temperature range, is defined as:

$$F_{in}(T) = 0.5 \cdot erfc\left(\frac{T - T_c}{T_{in}}\right), \quad (16)$$

where T is the in situ temperature, T_c is the threshold temperature, T_{in} the steepness parameter, and *erfc* the complementary error function (LaRowe et al., 2014).

We performed sensitivity tests using different values for the temperature coefficient for reactions rates Q_{10}, the steepness parameter T_{in} and the threshold temperature T_C for AOM and organic matter degradation (Fig. 3). Based on these tests, we have set the Q_{10} and T_{in}values to 1.7 and 1 °C, respectively. While $Q_{10} > 1.7$ leads to an even broader SMT, $Q_{10} < 1.7$ results in an upward shift of the deep SMT (Fig. 3A). High T_{in} values lead to a gradual decrease in and a smoothing of the temperature limiting term $F_{in}(T)$, which, in turn, would imply that microbial activity is not temperature-dependent (Fig. 3B).

Observations from cultivation-based approaches in hydrothermally influenced sediment from the Guaymas Basin demonstrated activity of thermophilic anaerobic methane-oxidizing communities at temperatures between 5 °C and 75 °C with an apparent optimum between 45 °C and 60 °C (Kallmeyer and Boetius, 2004; Holler et al., 2011). More recently, CH_4 at Site C0023 was found to be biologically oxidized until sediments reach a temperature of 80° to 85 °C. Using a T_C value for AOM greater than 60 °C, the SMT represents a sharp boundary (Fig. 3C). However, the CH_4 and SO_4^{2-} profiles currently overlap over a large interval of about 100 m (Fig. 2A). Therefore, we set the threshold temperature T_C=60 °C for AOM (Fig. S1M). Since vegetative cell concentrations and methanogenesis rates drop two orders of magnitude above 45 °C (Heuer et al., 2020), we use a T_C value of 45 °C for organic matter degradation (Fig. S1N-P). The temperature limiting term $F_{in}(T)$ is 1 when $T < T_C$ and approaches 0 when $T \geq T_C$.

The boundary conditions at the sediment-water interface are imposed concentrations and fluxes for the aqueous and solid species, respectively, while a zero-gradient boundary condition is used for all species at the sediment-basement interface. We used a constant domain size of 1200 m. Seven snapshots were constructed according to the age model for Site C0023 (Hagino and the Expedition 370 Scientists, 2018) with different sedimentation rates and C_{org} flux (F_{org1}, F_{org2} and F_{org3}) at the upper boundary at each depositional environment (Tab. S1).

The model was coded in R (version 3.2.4) using the ReacTran package (Soetaert and Meysman, 2012) to solve Eq. (1) and (2). The advective velocities of dissolved and solid species were solved using the compact grid function within the ReacTran package, which considers sediment compaction. All the species, parameters and boundary conditions except those given in the text are listed in Table S1.

3. Results and discussion

3.1. Past migration of the deep SMT

We simulated the evolution of the shallow and the deep SMT over the past 5.5 million years to quantitatively test the conceptual geochemical process model presented by Köster et al. (2021; Fig. 4). Low organic carbon supply and low sedimentation rates led to overall low carbon burial rates during deposition of the Lower Shikoku Basin facies. As a consequence, the C_{org} contents in these carbon-starved sediments were insufficient to deplete the entire SO_4^{2-} pool and consequently, it could penetrate deeply into the sediments (Köster et al., 2021). Our model confirms that SO_4^{2-} was not completely exhausted during deposition of the Lower Shikoku Basin facies but preserved in the lowermost 400 m (Fig. 4A). Increased C_{org} burial rates possibly related to elevated marine productivity during deposition of the Upper Shikoku Basin facies initiated the onset of biogenic methanogenesis (MG) ~2.5 million years ago (Ma). Consequently, a shallow SMT formed, where upward diffusing CH_4 reacted with SO_4^{2-} diffusing downwards from the overlying seawater. Due to the availability of the relict SO_4^{2-} pool in the Lower Shikoku Basin facies, a second deep inverse SMT formed, where downward diffusing CH_4 was oxidized by the preserved SO_4^{2-} (Fig. 4B; Köster

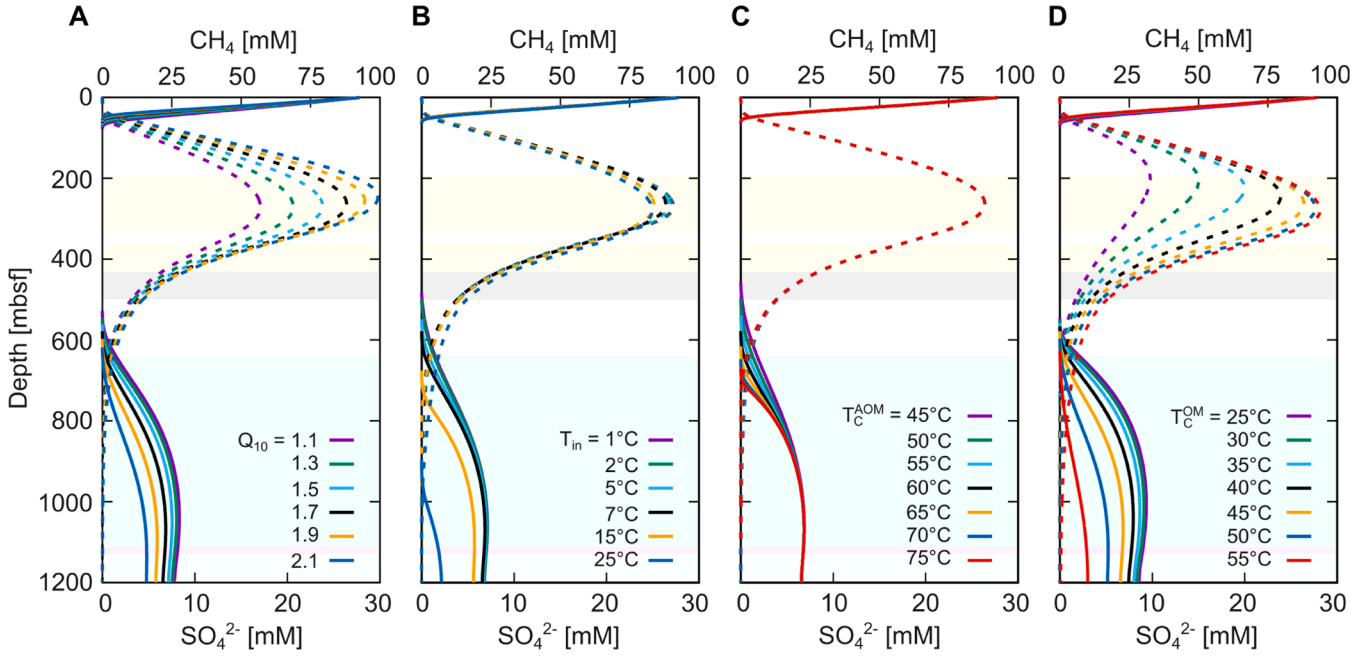

Fig. 3. Sensitivity tests using different values for Q_{10}, the steepness parameter T_{in} and the threshold temperature T_c for AOM and organic matter (OM) degradation. Solid and dashed lines represent sulfate (SO_4^{2-}) and methane (CH_4), respectively. In this study, we used $Q_{10} = 1.7$, $T_{in} = 1$ °C, $T_c = 60$ °C for AOM and $T_c = 45$ °C for organic matter degradation.

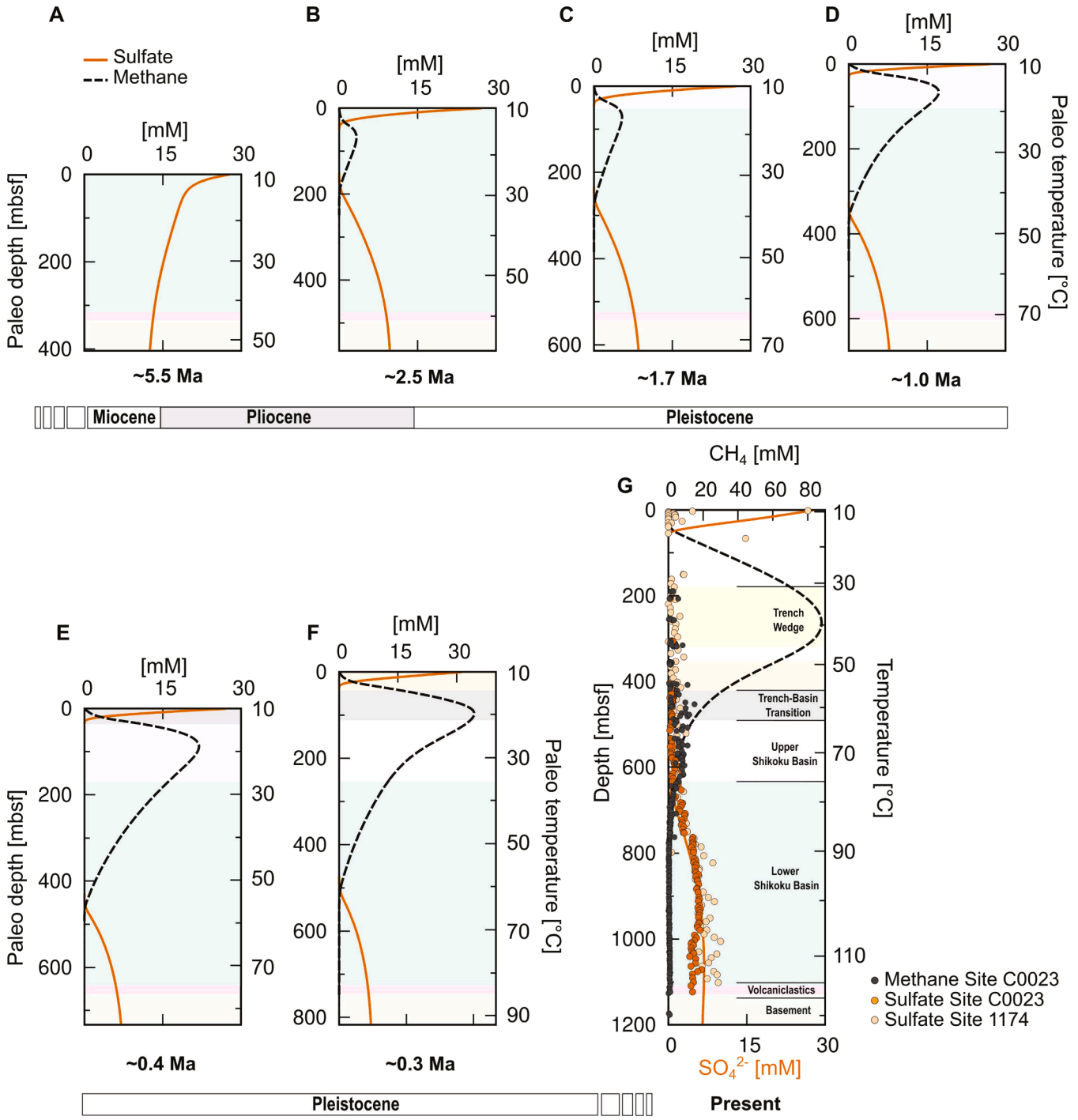

Fig. 4. Simulated profiles of sulfate (SO_4^{2-}) and methane (CH_4) derived from the reactive transport model over the past ~5.5 million years. The snapshots (A) to (F) correspond to the sedimentation intervals according to the age model for Site C0023 (Hagino and the Expedition 370 Scientists, 2018). (G) Present-day concentrations of SO_4^{2-} and CH_4 from IODP Site C0023 (Heuer et al., 2017) and SO_4^{2-} concentrations from ODP Site 1774 (Shipboard Science Party, 2001). Temperature data are from Heuer et al. (2020).

et al., 2021). Continuously increasing C_{org} burial resulted in elevated rates of methanogenesis. The resulting increased CH_4 fluxes shifted the shallow and deep SMTs up- and downwards, respectively (Fig. 4C). The formation of an inverse SMT and the subsequent migration as a consequence of changing C_{org} burial has earlier been described in subseafloor sediments from the Peruvian shelf (ODP Site 1229; Contreras et al., 2013) and in deep sediments from the Bering Sea (IODP Site U1341; Wehrmann et al., 2013). An increase in quantity and reactivity of C_{org} at Bowers Ridge in the Bering Sea, possibly linked to elevated surface primary productivity at around 2.6 Ma, led to elevated organoclastic sulfate reduction and initiated methanogenesis, followed by AOM and the development of two SMTs that migrated over ~130,000 years (Wehrmann et al., 2013). Similarly, variations in the supply and quality or C_{org} in response to glacial-interglacial cycles in sediments from the Peruvian shelf caused a cyclic 100,000-year migration of the SMT (Contreras et al., 2013). In contrast to subseafloor sediments from the Peruvian shelf and Bering Sea where the observed SMT dynamics are related to changes in C_{org} burial (Contreras et al., 2013; Wehrmann

et al., 2013), this study is the first to reconstruct the biogeochemical processes and microbial activity in deep subseafloor sediments as a function of both C_{org} burial and temperature by incorporating the temperature dependence into the reactive transport model.

Site C0023 entered the Nankai Trough ~0.4 Ma. The associated transition from hemipelagic basin- to trench-style deposition led to a pronounced increase in sedimentation rates by two orders of magnitude (Table 1; Hagino and the Expedition 370 Scientists, 2018). Since sediment temperature is a function of heat flow, thermal conductivity and depth below the seafloor, the arrival of Site C0023 in the trench is accompanied by a rapid ~50 °C increase of temperature across the entire sediment column (Horsfield et al., 2006; Heuer et al., 2020; Tsang et al., 2020). The significant heating of the sediments could have activated organic matter that is recalcitrant at seafloor temperatures of ~2–3 °C, thus bypassing extensive remineralization (e.g., Wellsbury et al., 1997; Burdige, 2011). Although the reactivation of recalcitrant organic matter at high temperatures was not included in the model, the simulated CH_4 profiles suggest enhanced CH_4 production in the methane-rich zone between 200 and 600 mbsf (Fig. 4F-G; Köster et al., 2021). The stable carbon isotopic composition of CH_4 ($\delta^{13}C$-CH_4) further supports this assumption. The $\delta^{13}C$-CH_4 values vary between −60 and −65‰ in the methane-rich zone, which is typical for a biogenic CH_4 source (Heuer et al., 2020). In contrast, the slight increase in CH_4 concentrations below the SMT (Fig. 2A) is attributable to thermogenic methane production (Heuer et al., 2017, 2020). Thermal degradation of organic matter, however, is not considered in the model.

3.2. Present-day sulfate and methane profiles and reaction rates

Our model reproduces the present-day SO_4^{2-} and CH_4 profile shapes (Fig. 4). Simulated CH_4 concentrations reach maximum values of ~90 mM at 250 mbsf. The current temperature at this depth is ~35 °C, which corresponds well with the optimum temperature for mesophilic microorganisms (20–43 °C) and the preferred temperature range of methanogens (35–42 °C; e.g., Zeikus and Winfrey, 1976). The offset between in situ and simulated CH_4 concentrations is caused by degassing that typically occurs during core recovery and sampling (e.g., Niewöhner et al., 1998). Gas voids that occur when the total gas pressure exceeds the confining pressure within the core liner (e.g., Spivack et al., 2006) were observed between 200 and 360 mbsf (Heuer et al., 2017), suggesting that in situ CH_4 concentrations were indeed higher than measured on board.

In this study, we derived present-day SR, biogenic MG and AOM rates from the reactive transport model (Fig. 5; Tab. S2). The modeled SR rates reach a maximum of almost 0.3 pmol cm^{-3} d^{-1} in the upper 100 mbsf (Fig. 5A). The MG rates are elevated between 100 and 400 mbsf with a maximum of ~0.4 pmol cm^{-3} d^{-1} (Fig. 5B). Potential SR and MG rates at Site C0023 were recently determined in radiotracer incubation experiments performed at different temperatures within the in situ range and the addition of different electron donors (Beulig et al., 2022). The potential SR and MG rates are extremely high (~10^2 to 10^3 pmol cm^{-3} d^{-1}) in incubations performed at 40 °C (between 200 and 400 mbsf), similar to the rates typically measured in shallow marine sediments. The SR and MG rates derived from our model are up to four orders of magnitude lower (Fig. 5A-B). Modeled rates that are orders of magnitude lower than those determined by radiotracer experiments are commonly observed and reported (e.g., Meister et al., 2022). Radiotracer incubations are usually carried out under idealized laboratory conditions. Although the incubation temperature was adjusted to the in situ temperature in the sediment, the pressure conditions do not correspond to the in situ conditions. Furthermore, the addition of different electron donors (trace H_2, acetate or CH_4) may have stimulated metabolic activity. Therefore, the reported rates represent the potential rather than the real metabolic activity of the microbial community (Beulig et al., 2022). While metabolic rates determined in radiotracer incubations are generally higher than in situ rates, our model includes assumptions that may lead to an underestimation of the actual metabolic rates. For example, since the temperature is an important factor regulating metabolic reaction rates (e.g., Arndt et al., 2013), we integrated a term that determines the temperature dependency of the rate constants $f(T)$ and the temperature-limiting term $F_{in}(T)$ for catabolic activity (LaRowe et al., 2014). We are aware that the rate constants may have an even more complex function of temperature, and thus, this approach may be greatly simplified. Although our modeled rates are significantly lower than the potential rates, they are similar to SR rates in other deep subseafloor environments. Both, modeled and potential SR rates in deep

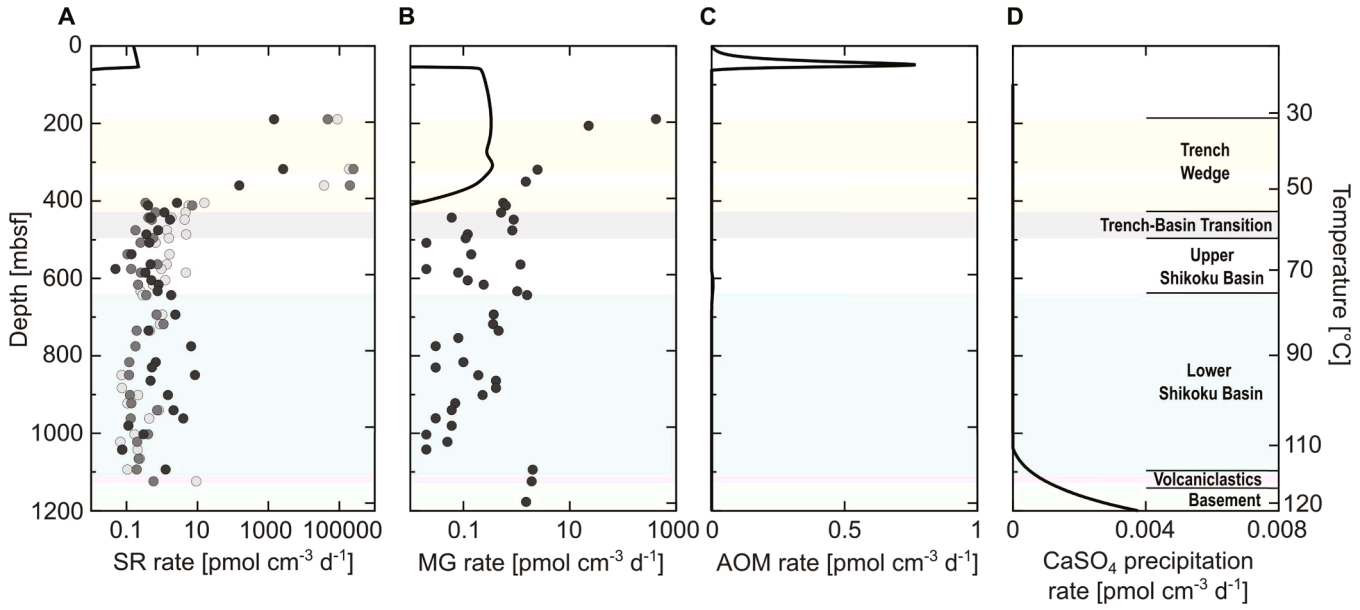

Fig. 5. Reaction rates derived from the reactive transport model. Simulated present-day rates of (A) organoclastic sulfate reduction (SR), (B) biogenic methanogenesis (MG), (C) anaerobic oxidation of methane (AOM) and (D) calcium sulfate ($CaSO_4$) precipitation. Black, dark grey and light grey dots in (A) indicate potential SR (using ^{35}S-SO_4^{2-}) with trace H_2, acetate and methane added, respectively (Beulig et al., 2022). Black dots in (B) indicate potential MG rates (using ^{14}C-DIC) (Beulig et al., 2022).

subseafloor sediments from the Peruvian shelf (ODP Leg 201), for example, range between 0.0001 and 0.1 pmol cm^{-3} d^{-1} (Tsang and Wortmann, 2022; Kallmeyer et al., 2025). Furthermore, SR rates derived from reaction transport modeling are in the range of 0.2 to 1.6 pmol cm^{-3} d^{-1} in deep sediments from the South Australian continental margin (ODP Site 1130, Leg 182; Wortmann, 2006). Additionally, radiotracer incubations performed at higher temperatures for Site C0023 (>400 mbsf) yield lower potential rates that are in a similar range to the rates derived from our model (<10 pmol cm^{-3} d^{-1}; Fig. 5A-B). Therefore, even if the potential and modeled rates for Site C0023 differ between 200 and 400 mbsf (Fig. 5A-B), the magnitude of our modeled rates are reasonable for deep subseafloor environments.

The significant downcore decrease in potential metabolic rates is accompanied by a drop in vegetative cells from $>10^4$ to $<10^2$ cells cm^{-3} at an in situ temperature between 40° and 50 °C (Heuer et al., 2020). This temperature range reflects the upper temperature limit for the mesophilic microbial community, suggesting that only (hyper-)thermophilic microorganisms survive burial into deeper and hotter sediments (Beulig et al., 2022).

Beulig et al. (2022) argued that SR has started ~0.4 Ma, following the onset of rapid sedimentation and associated heating of sediments. Their argumentation builds on the observation that at ODP Site 1225 in the eastern equatorial Pacific, where sediment age and C_{org} contents are similar to those at Site C0023, SO_4^{2-} is depleted by less than 2 mM compared to seawater values (Shipboard Scientific Party, 2003). However, thermal conditions at Site 1225 are markedly different with temperatures as low as 7 °C close to the basement. Based on our model, SR already occurred 5.5 Ma (Fig. 4A), when the thermal regime was similar compared to the upper ~400 m of the present-day sediment column and temperatures of up to 50 °C. This temperature range is consistent with the temperature optimum (~35 °C) of mesophilic sulfate-reducing bacteria (e.g., Isaksen and Jørgensen, 1996) and the maximum in potential SR rates in incubation experiments at 40 °C (Fig. 5A; Beulig et al., 2022). Pyrite enrichments accompanied by minima in magnetic susceptibility even in the lower parts of the Lower Shikoku Basin facies between 900 and 1100 mbsf suggest that the inverse SMT and the sulfidization front were located deeper in the past, which led to the diagenetic transformation of iron (oxyhydr)oxides into iron sulfides (Köster et al., 2021). Similar distinct sulfide-driven transformations of iron (oxyhydr)oxides into iron sulfides under non-steady-state diagenetic conditions have also been observed in continental margin sediments off Argentina and the Southeast African continent (Riedinger et al., 2005; März et al., 2008). Thus, an onset of organoclastic SR already during the deposition of the Lower Shikoku Basin facies before 0.4 Ma is plausible (Fig. 4).

The deep relict SO_4^{2-} shows a decrease below 1000 mbsf at temperatures above 105 °C, suggesting an additional sink of SO_4^{2-} (Fig. 2A). The concomitant sharp increase in Ca^{2+} concentration from 50 to 170 mM near the basement (Fig. 2C) can be attributed to plagioclase alteration in the basement (Heuer et al., 2017). During this albitization, anorthite ($CaAl_2Si_2O_8$) is replaced by albite ($NaAl_2Si_3O_8$) and Ca^{2+} is released into the pore water (e.g., Humphris and Thompson, 1978). The overall decrease in SO_4^{2-} below 1000 mbsf could be due to the precipitation of anhydrite ($CaSO_4$), a major sink for SO_4^{2-} in hydrothermal systems (e.g., Alt et al., 1986). We integrated the precipitation of $CaSO_4$ phases in the reactive transport model and derived the precipitation rate (Fig. 5D). It is important to note here that Ca^{2+} concentrations were not directly calculated and carbonate precipitation was neglected. We are aware that the implementation of carbonate and dolomite precipitation, for example, will significantly alter the pore-water profiles of DIC and SO_4^{2-} (Fig. S1). The implementation of anhydrite precipitation in our model is intended solely as an example of how further processes can be incorporated, especially under high temperature conditions. The pore water is saturated with respect to anhydrite below 1000 mbsf above 110 °C. Consequently, the model reproduces a slight decrease in SO_4^{2-} concentrations in the deeper core (Fig. 4G). Anhydrite precipitation accounts for almost 1 % of the total SO_4^{2-} consumption (Fig. 6).

The current depth of the shallow SMT at Site C0023 could not be determined during IODP Expedition 370 since sediments shallower than ~200 mbsf were not recovered (Heuer et al., 2017). Based on SO_4^{2-} and CH_4 profiles from the adjacent ODP Site 1174 (Shipboard Scientific Party, 2001), we assume that the shallow SMT is located at ~5 mbsf. The simulated SMT, however, is located at around 50 mbsf (Fig. 4G). This difference is related to the lack of geochemical and sedimentation rate data in the upper 200 m of the sediment column. Therefore, we used the sedimentation rate of the Trench Wedge facies and took C_{org} data as fitting parameter for the upper 200 m in the model. We performed a time series simulation for the upward migration of the shallow SMT (Fig. 7). If assuming a constant present-day sedimentation rate of ~130 cm kyr^{-1} similar to the rate in the most recent Trench Wedge facies (Hagino and the Expedition 370 Scientists, 2018), an increase in C_{org} contents of up to 4 wt % in the upper 30 m of the sediment column is necessary to shift the shallow SMT to ~7 mbsf. This upward migration will take around 2000 years (Fig. 7A). An overall increase in C_{org} contents is reasonable due to the proximity to the Japanese Islands (Fig. 1) and, hence, a related higher input of (terrigenous) organic-rich material from the coast at the shelf off Shikoku Island. However, an increase of up to 4 wt % might be overestimated. Thus, we suspect that the shallow position of the SMT is likely the result of increasing C_{org} contents in the surface sediments, but at the same time, a decrease in present-day sedimentation rates compared to a rate of ~130 cm kyr^{-1}.

3.3. Fading of the deep inverse SMT

In marine shelf sediments, the SMT is commonly considered as a sharp boundary where SO_4^{2-} and CH_4 concentrations decrease below detection limit (e.g., Niewöhner et al., 1998; Riedinger et al., 2005). At Site C0023, the SO_4^{2-} and CH_4 profiles overlap in a relatively broad zone between ~600 and 700 mbsf, whereby CH_4 only reaches near-zero concentrations (<0.5 mM) at ~785 mbsf (Fig 2A). A similar tailing of CH_4 into the SO_4^{2-}-rich zone, but at considerably shallower depth of 2 to 3 mbsf, has been commonly observed in shallow sediments of the Black Sea and is explained by inefficient microbial CH_4 oxidation (e.g., Knab et al., 2009). A positive excursion in $\delta^{13}C$-CH_4 values up to −54‰, indicative of a biogenic CH_4 sink and the activity of AOM-performing organisms (Heuer et al., 2020), locates the current deep inverse SMT at ~730 mbsf and, thus, between the actual sulfate-methane overlap zone and the depth, where CH_4 decreases to near-zero (~785 mbsf). This depth corresponds to a temperature of 80° to 85 °C (Fig. 2A). As

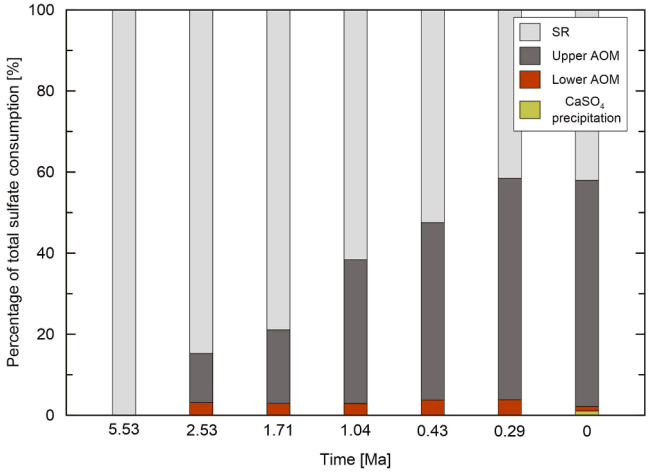

Fig. 6. Percentage of organoclastic sulfate reduction (SR), anaerobic oxidation of methane (AOM) and anhydrite ($CaSO_4$) precipitation in the total sulfate consumption over the past ~5.5 Ma. Upper and lower AOM correspond to the consumption at the shallow and the deep inverse SMT, respectively.

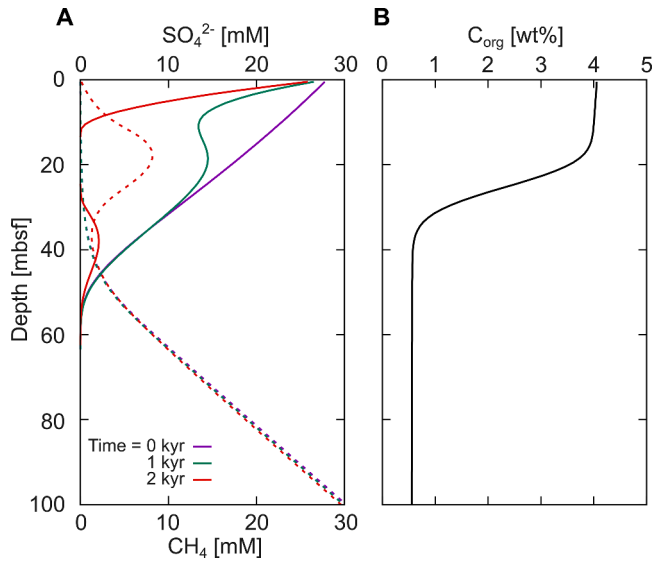

Fig. 7. Time series for the evolution of the sulfate (SO_4^{2-}; solid lines) and methane (CH_4; dashed lines) profiles if the C_{org} contents in the upper ~30 m of the sediment column are increased of up to 4 wt %. The sedimentation rate in this scenario is equal to the sedimentation rate of ~130 cm kyr^{-1} determined for the most recent Trench Wedge facies recovered at Site C0023.

incubation experiments with hydrothermal sediments from the Guaymas Basin have shown that AOM is limited at temperatures around 80 °C (e.g., Kallmeyer and Boetius, 2004; Holler et al., 2011), Köster et al. (2021) inferred that AOM only barely occurs at Site C0023 at present.

Here, we assess the evolution of AOM activity by simulating AOM rates. The depth-integrated AOM rate for the inverse SMT significantly dropped from ~0.45 to 0.1 mmol m^{-2} yr^{-1} since the beginning of the rapid burial and associated heating of sediments ~0.4 Ma (Fig. 8). Similarly, the isotopic composition of dissolved inorganic carbon (δ^{13}C-DIC) provides no indication of intense AOM activity at the present-day inverse SMT (Fig. 2B). Strongly ^{13}C-depleted DIC down to −30.0‰ is typically indicative of AOM (e.g., Alperin et al., 1988; Meister and Reyes, 2019). At Site C0023, δ^{13}C-DIC values are relatively constant around -5.0‰ below 500 mbsf. Furthermore, the potential AOM and SR rates with the excess addition of CH_4 are not elevated at the depth of the current deep SMT (Beulig et al., 2022). These observations collectively suggest that AOM activity at the inverse SMT is at the threshold to cease or has already stopped and consequently, the SMT is in the process of gradually disappearing. This is consistent with the findings of a previous study in which we demonstrated that, based on the isotopic composition of dissolved iron, the microbially mediated release of iron stopped due to the increase in temperature beyond the threshold of mesophilic microorganism (Köster et al., 2023). In the future, the concentration gradients of SO_4^{2-} and CH_4 will further equilibrate by diffusion, leading to an even broader sulfate-methane overlap zone. Such extremely broad overlap zones of SO_4^{2-} and CH_4, for example, have been observed at the open-ocean ODP Site 1226 in the eastern Pacific Ocean, which is characterized by low C_{org} contents and net metabolic rates (D'Hondt et al., 2004) or at ODP Site 1131 on the continental margin of the Great Australian Bight (Mitterer et al., 2001). The process described here for Site C0023 is referred to a "fading SMT". This is the first time that such a fading of an SMT due to cessation of microbial activity has been observed in situ close to the temperature limit of the deep biosphere. In summary, compared to other deep subseafloor environments, Site C0023 has two notable characteristics, highlighting its unique biogeochemistry. Firstly, a deep inverse SMT is often associated with SO_4^{2-} diffusion from the underlying basement aquifer (e.g., D'Hondt et al., 2004; Torres et al., 2015; Zindorf et al., 2019; Tsang and Wortmann, 2022). Sulfate in the deep sediments at Site C0023, however, is the result of a relict pool, that was not completely exhausted during deposition of the Lower Shikoku Basin facies (Köster et al., 2021). Secondly, while the inverse SMT in relatively cold subseafloor environments (e.g., Peruvian shelf) is controlled by C_{org} burial, the SMT dynamics at Site C0023 are governed by the combination of changing C_{org} burial and increasing sediment temperature.

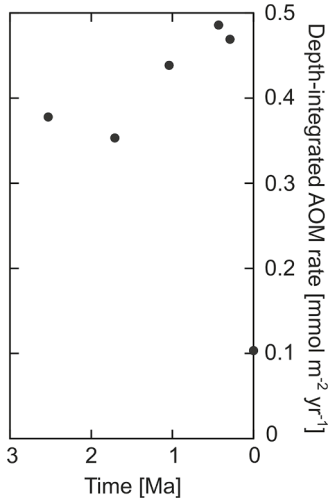

Fig. 8. Simulated depth-integrated AOM rate since the onset of AOM 2.5 Ma.

4. Conclusions

In this study, we quantitatively tested the conceptual model we previously proposed (Köster et al., 2021) by using reactive transport modeling. Site C0023 has undergone significant changes in biogeochemical processes, which are ultimately the result of strongly changing depositional and, in particular, thermal conditions that are driven by the tectonic migration of the ocean floor. Based on the reactive transport model, we demonstrated the evolution of the deep inverse SMT from its formation at ~2.5 Ma, through its downward migration until ~0.5 Ma, to its decay since the onset of the rapid heating at ~0.4 Ma. With progressive burial and associated heating, the AOM activity at the deeper inverse SMT gradually decreases and the SMT successively disappears. Our study demonstrates that the sediment temperature plays a key factor in determining the rates of biogeochemical processes and microbial activity – in particular in deposits of subduction zones like the Nankai Trough and the Cascadia margin that are characterized by high geothermal gradients. Therefore, changes in temperature and their impact on rate constants as a consequence of the local burial history of such sediments should be considered in order to improve the reconstruction of pore-water and sedimentary records.

Overall, our study contributes to an improved understanding of the variability of biogeochemical processes and microbial activity in deep subseafloor sediments over geological timescales. It further demonstrates that the geochemical patterns (i.e. pore-water profiles and sedimentary record) we observe today are a consequence of long-term variations in depositional conditions, the organic carbon availability and temperature conditions.

Data availability

The data generated in this study (isotopic composition of dissolved inorganic carbon (δ^{13}C-DIC)) are archived in the World Data Center PANGAEA via https://doi.pangaea.de/10.1594/PANGAEA.971450 (Köster et al., 2025). All other data relevant for this study are also available in the data repository PANGAEA via https://doi.org/10.1594/PANGAEA.889808 (Pore-water data; Heuer et al., 2018a) and https://doi.org/10.1594/PANGAEA.889721 (Sediment data; Heuer

et al., 2018b) or reported in the Expedition Report (https://doi.org/10.14379/iodp.proc.370.103.2017; Heuer et al., 2017).

CRediT authorship contribution statement

Male Köster: Writing – review & editing, Writing – original draft, Visualization, Investigation, Conceptualization. **Bo Liu:** Writing – review & editing, Visualization, Investigation, Formal analysis. **Akira Ijiri:** Writing – review & editing. **Arthur J. Spivack:** Writing – review & editing. **Yuki Morono:** Writing – review & editing. **Fumio Inagaki:** Writing – review & editing. **Verena B. Heuer:** Writing – review & editing. **Sabine Kasten:** Writing – review & editing, Supervision, Conceptualization. **Susann Henkel:** Writing – review & editing, Supervision, Project administration, Funding acquisition, Conceptualization.

Declaration of competing interest

The authors declare that they have no known competing financial interests or personal relationships that could have appeared to influence the work reported in this paper.

Acknowledgements

This research used samples and data provided by the International Ocean Discovery Program (IODP). We thank all personnel involved in operations onboard the *D/V Chikyu*, especially Kira Homola and Justine Sauvage, and in the Kochi Core Center during Expedition 370. This study is funded by the German Research Foundation (DFG) in the framework of the priority program (SPP) 527 (project 388260220). Bo Liu received financial support from the BMBF MARE:N project "Anthropogenic impacts on particulate organic carbon cycling in the North Sea (APOC)" (grant no. 03F0874A). We acknowledge further financial support from the Helmholtz Association. This study received further funding by the Federal Agency for Nature Conservation (BfN) as part of the Federal Action Plan on Nature-based Solutions for Climate and Biodiversity with funds from the German Federal Ministry for the Environment, Climate Action, Nature Conservation and Nuclear Safety (BMUKN) in the framework of the Cooperation KomSO "Studie zur Kohlenstoffspeicherkapazität mariner Sedimente in der deutschen Ostsee" (FKZ 3523NK370A-E). Finally, the authors thank the editor and three anonymous reviewers for their helpful and constructive comments, which have significantly improved this manuscript.

Supplementary materials

Supplementary material associated with this article can be found, in the online version, at doi:10.1016/j.epsl.2025.119694.

References

Alperin, M.J., Reeburgh, W.S., Whiticar, M.J., 1988. Carbon and hydrogen isotope fractionation resulting from anaerobic methane oxidation. Global Biogeochem. Cy. 2, 279–288. https://doi.org/10.1029/GB002i003p00279.

Alt, J.C., Honnorez, J., Laverne, C., Emmermann, R., 1986. Hydrothermal alteration of a 1 km section through the upper oceanic crust, Deep Sea Drilling Project Hole 504B: mineralogy, chemistry and evolution of seawater-basalt interactions. J. Geophys. Res. Solid Earth 91, 10309–10355. https://doi.org/10.1029/JB091iB10p10309.

Arndt, S., Brumsack, H.-J., Wirtz, K.W., 2006. Cretaceous black shales as active bioreactors: a biogeochemical model for the deep biosphere encountered during ODP Leg 207 (Demera Rise). Geochim. Cosmochim. Acta 70, 408–425. https://doi.org/10.1016/j.gca.2005.09.010.

Arndt, S., Jørgensen, B.B., LaRowe, D.E., Middelburg, J.J., Pancost, R.D., Regnier, R., 2013. Quantifying the degradation or organic matter in marine sediments: a review and synthesis. Earth-Sci. Rev. 123, 53–86. https://doi.org/10.1016/j.earscirev.2013.02.008.

Berner, R.A., 1980. Early diagenesis: A theoretical Approach. Princeton University Press, Princeton, New Jersey.

Beulig, F., Schubert, F., Adhikari, R.R., Glombitza, C., Heuer, V.B., Hinrichs, K.-U., Homola, K.L., Inagaki, F., Jørgensen, B.B., Kallmeyer, J., Krause, S.J.E., Morono, Y., Sauvage, J., Spivack, A.J., Treude, T., 2022. Rapid metabolism fosters microbial survival in deep, hot subseafloor biosphere. Nat. Commun. 13, 312. https://doi.org/10.1038/s41467-021-27802-7.

Blöchl, E., Rachel, R., Burggraf, S., Hafenbradl, D., Janasch, H.W., Stetter, K.O., 1997. *Pyrolobus fumarii*, gen. And sp. nov., represents a novel group of archaea, extending the upper temperature limit for live to 113 °C. Extremophiles 1, 14–21. https://doi.org/10.1007/s007920050010.

Boudreau, B.P., 1996. The diffusive tortuosity of fine-grained unlithified sediments. Geochim. Cosmochim. Acta. 60, 3139–3142. https://doi.org/10.1016/0016-7037(96)00158-5.

Boudreau, B.P., 1997. A one-dimensional model for bed-boundary layer particle exchange. J. Mar. Syst 11, 279–303. https://doi.org/10.1016/S0924-7963(96)00127-3.

Burdige, D.J., 2011. Temperature dependence of organic matter remineralization in deeply-buried marine sediments. Earth Planet. Sci. Lett. 311, 396–410. https://doi.org/10.1016/j.epsl.2011.09.043.

Burdige, D.J., Komada, T., Magen, C., Chanton, J.P., 2016a. Carbon cycling in Santa Barbara Basin sediments: a modeling study. J. Mar. Res. 74, 133–159. https://doi.org/10.1357/002224016819594818.

Burdige, D.J., Komada, T., Magen, C., Chanton, J.P., 2016b. Methane dynamics in Santa Barbara Basin (USA) sediments as examined with a reaction-transport model. J. Mar. Res. 74, 277–313. https://doi.org/10.1357/002224016821744151.

Contreras, S., Meister, P., Liu, B., Prieto-Mollar, X., Hinrichs, K.-U., Khalili, A., Ferdelman, T.G., Kuypers, M.M.M., Jørgensen, B.B., 2013. Cyclic 100-ka (glacial-interglacial) migration of subseafloor redox zonation on the Peruvian shelf. Proc. Natl. Acad. Sci 110, 18098–18103. https://doi.org/10.1073/pnas.1305981110.

D'Hondt, S., Rutherford, S., Spivack, A.J., 2002. Metabolic activity of subsurface life in deep-sea sediments. Science 295, 2067–2070. https://doi.org/10.1126/science.1064878.

D'Hondt, S., Jørgensen, B.B., Miller, D.J., Batzke, A., Blake, R., Cragg, B.A., Cypionka, H., Dickens, G.R., Ferdelman, T., Hinrichs, K.-U., Holm, N.G., Mitterer, R., Spivack, A., Wang, G., Bekins, B., Engelen, B., Ford, K., Gettemy, G., Rutherford, S.D., Sass, H., Skilbeck, C.G., Aiello, I.W., Guèrin, G., House, C.H., Inagaki, F., Meister, P., Naehr, T., Niitsuma, S., Parkes, R.J., Schippers, A., Smith, D.D., Teske, A., Wiegel, J., Padilla, C.N., Acosta, J.L., 2004. Distributions of microbial activities in deep subseafloor sediments. Science 306, 2216–2221. https://doi.org/10.1126/science.1101155.

Hagino, K., 2018. Data report: calcareous nannofossils from the middle miocene to pleistocene, IODP Expedition 370 site C0023. Heuer, V.B., Inagaki, F., Morono, Y., Kubo, Y., Maeda, L., and the Expedition 370 Scientists. In: Temperature Limit of the Deep Biosphere Off Muroto, Proceedings of the International Ocean Discovery Program, 370. International Ocean Discovery Program, College Station, TX. https://doi.org/10.14379/iodp.proc.370.201.2018.

Henkel, S., Mogollón, J.M., Nöthen, K., Franke, C., Bogus, K., Robin, E., Bahr, A., Blumenberg, M., Pape, T., Seifert, R., März, C., de Lange, G.J., Kasten, S., 2012. Diagenetic barium cycling in Black Sea sediments – A case study for anoxic marine environments. Geochim. Cosmochim. Acta. 88, 88–105. https://doi.org/10.1016/j.gca.2012.04.021.

Heuer, V.B., Inagaki, F., Morono, Y., Kubo, Y., Maeda, L., 2017. Temperature limit of the deep biosphere off Muroto. In: Proceedings of the International Ocean Discovery Program, 370. International Ocean Discovery Program, College Station, TX. https://doi.org/10.14379/iodp.proc.370.2017.

Heuer, V.B., Inagaki, F., Morono, Y., Kubo, Y., Maeda, L., 2018a. Chemistry Measurements of Pore Water from IODP Hole 370-C0023A. PANGAEA. https://doi.org/10.1594/PANGAEA.889808. Dataset.

Heuer, V.B., Inagaki, F., Morono, Y., Kubo, Y., Maeda, L., 2018b. CNS-analysis from IODP Hole 370-C0023A. PANGAEA. https://doi.org/10.1594/PANGAEA.889721. Dataset.

Heuer, V.B., Inagaki, F., Morono, Y., Kubo, Y., Spivack, A.J., Viehweger, B., Treude, T., Beulig, F., Schubotz, F., Tonai, S., Bowden, S.A., Cramm, M., Henkel, S., Hirose, T., Homola, K., Hoshino, T., Ijiri, A., Imachi, H., Kamiya, N., Kaneko, M., Lagostina, L., Manners, H., McClelland, H.-L., Metcalfe, K., Okutsu, N., Pan, D., Raudsepp, M.J., Sauvage, S., Tsang, M.-Y., Wang, D.T., Whitaker, E., Yamamoto, Y., Yang, K., Maeda, L., Adhikari, R.R., Glombitza, C., Hamada, Y., Kallmeyer, J., Wendt, J., Wörmer, L., Yamada, Y., Kinoshita, M., Hinrichs, K.-U., 2020. Temperature limits to deep subseafloor life in the Nankai Trough subduction zone. Science 370, 1230–1234. https://doi.org/10.1126/science.abd7934.

Holler, T., Widdel, F., Knittel, K., Amann, R., Kellermann, M.Y., Hinrichs, K.-U., Teske, A., Boetius, A., Wegener, G., 2011. Thermophilic anaerobic oxidation of methane by marine microbial consortia. ISME J 5, 1946–1956. https://doi.org/10.1038/ismej.2011.77.

Hoshino, T., Doi, H., Uramoto, G.-I., Wörmer, L., Adhikari, R.R., Xiao, N., Morono, Y., D'Hondt, S., Hinrichs, K.-U., Inagaki, F., 2020. Global diversity of microbial communities in marine sediment. Proc. Natl. Acad. Sci. 117, 27587–27597. https://doi.org/10.1073/pnas.1919139117.

Horsfield, B., Schenk, H.J., Zink, K., Ondrak, R., Dieckmann, V., Kallmeyer, J., Mangelsdorf, K., di Primio, R., Wilkes, H., Parkes, R.J., Fry, J., Cragg, B., 2006. Living microbial ecosystems within the active zone of catagenesis: implications for feeding the deep biosphere. Earth Planet. Sci. Lett. 246, 55–69. https://doi.org/10.1016/j.epsl.2006.03.040.

Humphris, S.E., Thompson, G., 1978. Hydrothermal alteration of oceanic basalts by seawater. Geochim. Cosmochim. Acta. 42, 107–125. https://doi.org/10.1016/0016-7037(78)90221-1.

Ijiri, A., Harada, N., Hirota, A., Tsunogai, U., Ogawa, N.O., Itaki, T., Khim, B.-K., Uchida, M., 2012. Biogeochemical processes involving acetate in sub-seafloor sediments from the Bering Sea shelf break. Org. Geochem. 48, 47–55. https://doi.org/10.1016/j.orggeochem.2012.04.004.

Inagaki, F., Hinrichs, K.-U., Kubo, Y., Bowles, M.W., Heuer, V.B., Hong, W.-L., Hoshino, T., Ijiri, A., Imachi, H., Ito, M., Kaneko, M., Lever, M.A., Lin, Y.-S., Methé, B.A., Morita, S., Morono, Y., Tanikawa, W., Bihan, M., Bowden, S.A., Elvert, M., Glombitza, C., Gross, D., Harrington, G.J., Hori, T., Li, K., Limmer, D., Liu, C.-H., Murayama, M., Ohkouchi, N., Ono, S., Park, Y.-S., Phillips, S.C., Prieto-Mollar, X., Purkey, M., Riedinger, N., Sanada, Y., Sauvage, J., Snyder, G., Susilawati, R., Takano, Y., Tsaumi, E., Terada, T., Tomaru, H., Trembath-Reichert, E., Wang, D.T., Yamada, Y., 2015. Exploring deep microbial life in coal-bearing sediment down to ~2.5 km below the ocean floor. Science 349, 420–424. https://doi.org/10.1126/science.aaa6882.

Inagaki, F., Nunoura, T., Nakagawa, S., Teske, A., Lever, M., Lauer, A., Suzuki, M., Takai, K., Delwiche, M., Colwell, F.S., Nealson, K.H., Horikoshi, K., D'Hondt, S., Jørgensen, B.B., 2006. Biogeographical distribution and diversity of microbes in methane hydrate-bearing deep marine sediments on the Pacific Ocean Margin. Proc. Natl. Acad. Sci. 103, 2815–2820. https://doi.org/10.1073/pnas.0511033103.

Isaksen, M.F., Jørgensen, B.B., 1996. Adaptation of psychrophilic and psychrotrophic sulfate-reducing bacteria to permanently cold marine environments. Appl. Environ. Microbiol. 62, 408–414. https://doi.org/10.1128/aem.62.2.408-414.1996.

Jørgensen, B.B., 1978. A comparison of methods for the quantification of bacterial sulfate reduction in coastal marine sediments: II. Calculation from mathematical models. Geomicrobiol. J. 1, 11–27. https://doi.org/10.1080/01490457809377722.

Kallmeyer, J., Boetius, A., 2004. Effects of temperature and pressure on sulfate reduction and anaerobic oxidation of methane in hydrothermal sediments of Guaymas Basin. Appl. Environ. Microbiol. 70, 1231–1233. https://doi.org/10.1128/AEM.70.2.1231-1233.2004.

Kallmeyer, J., Pockalny, R., Adhikari, R.R., Smith, D.C., D'Hondt, S., 2012. Global distribution of microbial abundance and biomass in subseafloor sediment. Proc. Natl. Acad. Sci. 109, 16213–16216. https://doi.org/10.1073/pnas.1203849109.

Kallmeyer, J., Ferdelman, T.G., Liu, B., Parkes, R.J., Røy, H., Jørgensen, B.B., 2025. Sulfate reduction rates in Peru margin sediments: from 1 cm to 100 m below seafloor. Geochim. Cosmochim. Acta. 399, 111–124. https://doi.org/10.1016/j.gca.2025.04.019.

Kasten, S., Freudenthal, T., Gingele, F.X., Schulz, H.D., 1998. Simultaneous formation of iron-rich layers at different redox boundaries in sediments of the Amazon deep-sea fan. Geochim. Cosmochim. Acta. 62, 2253–2264. https://doi.org/10.1016/S0016-7037(98)00093-3.

Knab, N.J., Cragg, B.A., Hornibrook, E.R.C., Holmkvist, L., Pancost, R.D., Borowski, C., Parkes, R.J., Jørgensen, B.B., 2009. Regulation of anaerobic methane oxidation in sediments of the Black Sea. Biogeosciences 6, 1505–1518. https://doi.org/10.5194/bg-6-1505-2009.

Köster, M., Kars, M., Schubotz, F., Tsang, M.-Y., Maisch, M., Kappler, A., Morono, Y., Inagaki, F., Heuer, V.B., Kasten, S., Henkel, S., 2021. Evolution of (bio)geochemical processes and diagenetic alteration of sediments along the tectonic migration of ocean floor in the Shikoku Basin off Japan. Geochem. Geophys. Geosyst. 22, e2020GC009585. https://doi.org/10.1029/2020GC009585.

Köster, M., Staubwasser, M., Meixner, A., Kasemann, S.A., Manners, H.R., Morono, Y., Inagaki, F., Heuer, V.B., Kasten, S., Henkel, S., 2023. Uniquely low stable iron isotopic signatures in deep marine sediments caused by Rayleigh distillation. Sci. Rep. 13, 10281. https://doi.org/10.1038/s41598-023-37254-2.

Köster, M., Liu, B., Ijiri, A., Spivack, A.J., Morono, Y., Inagaki, F., Heuer, V.B., Kasten, S., Henkel, S.. Carbon isotopic composition of dissolved inorganic carbon (δ13C-DIC) at IODP Site 370-C0023, Nankai Trough subduction zone [dataset]. https://doi.pangaea.de/10.1594/PANGAEA.971450.

LaRowe, D.E., Dale, A.W., Aguilera, D.R., L'Heureux, I., Amend, J.P., Regnier, P., 2014. Modeling microbial reaction rates in a submarine hydrothermal vent chimney wall. Geochim. Cosmochim. Acta 124, 72–97. https://doi.org/10.1016/j.gca.2013.09.005.

Lever, M.A., Rogers, K.L., Lloyd, K.G., Overmann, J., Schink, B., Thauer, R.K., Hoehler, T. M., Jørgensen, B.B., 2015. Life under extreme energy limitations: a synthesis of laboratory- and field-based investigations. FEMS Microbiol. Rev. 39, 688–728. https://doi.org/10.1093/femsre/fuv020.

Lin, W., Byrne, T.B., Kinoshita, M., McNeill, L.C., Chang, C., Lewis, J.C., Yamamoto, Y., Saffer, D.M., Moore, J.C., Wu, H.-Y., Tsuji, T., Yamada, Y., Conin, M., Saito, S., Ito, T., Tobin, H.J., Kimura, G., Kanagawa, K., Ashi, J., Underwood, M.B., Kanamatsu, T., 2016. Distribution of stress state in the Nankai subduction zone, southwest Japan and a comparison with Japan Trench. Tectonophysics 692, 120–130. https://doi.org/10.1016/j.tecto.2015.05.008.

Mahony, S.H., Wallace, L.M., Miyoshi, M., Villamor, P., Sparks, R.S.J., Hasenaka, T., 2011. Volcano-tectonic interactions during rapid plate-boundary evolution in the Kyushu region, SW Japan. Geol. Soc. Am. Bull. 123, 2201–2223. https://doi.org/10.1130/B30408.1.

März, C., Hoffmann, J., Bleil, U., de Lange, G.J., Kasten, S., 2008. Diagenetic changes of magnetic and geochemical signals by anaerobic methane oxidation in sediments of the Zambezi deep-sea fan (SW Indian Ocean). Mar. Geol. 255, 118–130. https://doi.org/10.1016/j.margeo.2008.05.013.

Meister, P., Brunner, B., Picard, A., Böttcher, M.E., Jørgensen, B.B., 2019. Sulphur and carbon isotopes as tracers of past sub-seafloor microbial activity. Sci. Rep. 9, 1–9. https://doi.org/10.3390/geosciences9120507.

Meister, P., Herda, G., Petrishcheva, E., Gier, S., Dickens, G.R., Bauer, C., Liu, B., 2022. Microbial alkalinity production and silicate alteration in methane charged marine sediments: implication for porewater chemistry and diagenetic carbonate formation. Front. Earth Sci. 9, 756591. https://doi.org/10.3389/feart.2021.756591.

Mitterer, R.M., Malone, M.J., Goodfriend, G.A., Swart, P.K., Wortmann, U.G., Logan, G. A., Feary, D.A., Hine, A.C., 2001. Co-generation of hydrogen sulfide and methane in marine carbonate sediments. Geophys. Res. Lett. 28, 3932–3934. https://doi.org/10.1029/2001GL013320.

Mogollón, J.M., Mewes, K., Kasten, S., 2016. Quantifying manganese and nitrogen cycle coupling in manganese-rich, organic carbon-starved marine sediments: examples from the Clarion-Clipperton fracture zone. Geophys. Res. Lett. 43, 7114–7123. https://doi.org/10.1002/2016GL069117.

Morono, Y., Inagaki, F., Heuer, V.B., Kubo, Y., Maeda, L., 2017. Expedition 370 methods. Heuer, V.B., Inagaki, F., Morono, Y., Kubo, Y., Maeda, L., and the Expedition 370 Scientists. In: Temperature Limit of the Deep Biosphere Off Muroto, Proceedings of the International Ocean Discovery Program, 370. (International Ocean Discovery Program), College Station, TX. https://doi.org/10.14379/iodp.proc.370.102.2017.

Nauhaus, K., Boetius, A., Krüger, M., Widdel, F., 1995. In vitro demonstration of anaerobic oxidation of methane coupled to sulphate reduction in sediment from a marine gas hydrate area. Environ. Microbiol. 4, 296–305. https://doi.org/10.1046/j.1462-2920.2002.00299.x.

Niewöhner, C., Hensen, C., Kasten, S., Zabel, M., Schulz, H.D., 1998. Deep sulfate reduction completely mediated by anaerobic methane oxidation in sediments of the upwelling area off Namibia. Geochim. Cosmochim. Acta. 62, 455–464. https://doi.org/10.1016/S0016-7037(98)00055-6.

Riedinger, N., Pfeifer, K., Kasten, S., Garming, J.F.L., Vogt, C., Hensen, C., 2005. Diagenetic alteration of magnetic signals by anaerobic oxidation of methane related to a change in sedimentation rate. Geochim. Cosmochim. Acta. 69, 4117–4126. https://doi.org/10.1016/j.gca.2005.02.004.

Shipboard Scientific Party, 2001. Site 1174. In: Moore, G.F., Taira, A., Klaus, A. (Eds.), Proceedings of Ocean Drilling Program, Initial Reports, Volume 190. College Station, TX (Ocean Drilling Program), pp. 1–149. https://doi.org/10.2973/odp.proc.ir.190.105.2001.

Shipboard Scientific Party, 2003. Site 1225. In: D'Hondt, S., Jørgensen, B.B., Miller, D.J., et al. (Eds.), Proceedings of Ocean Drilling Program, Initial Reports, Volume 201. College Station, TX (Ocean Drilling Program), pp. 1–86. https://doi.org/10.2973/odp.proc.ir.201.106.2003.

Soetaert, K., Meysman, F., 2012. Reactive transport in aquatic ecosystems: rapid model prototyping in the open source software R. Environ. Model. Softw. 32, 49–60. https://doi.org/10.1016/j.envsoft.2011.08.011.

Spivack, A.J., McNeil, C., Holm, N.G., Hinrichs, K.-U., et al., 2006. Determination of in situ methane based on analysis of void gas. In: Jørgensen, B.B., D'Hondt, S.L., Miller, D.J., et al. (Eds.), Proceedings of Ocean Drilling Program, Scientific Results, 201. https://doi.org/10.2973/odp.proc.sr.201.119.2006.

Taira, A., Hill, I., Firth, J., Berner, U., Brückmann, W., Byrne, T., Chabernaud, T., Fisher, A., Foucher, J.-P., Gamo, T., Gieskes, J., Hyndman, R., Karig, D., Kastner, M., Kato, Y., Lallemant, S., Lu, R., Maltman, A., Moore, G., Moran, K., Olaffson, G., Owens, W., Pickering, K., Siena, F., Taylor, E., Underwood, M., Wilkinson, C., Yamano, M., Zhang, J., 1992. Sediment deformation and hydrogeology of the Nankai Trough accretionary prism: synthesis of shipboard results of ODP Leg 131. Earth Planet. Sci. Lett. 109, 431–450. https://doi.org/10.1016/0012-821X(92)90104-4.

Takai, K., Nakamura, K., Toki, T., Tsunogai, U., Miyazaki, M., Miyazaki, J., Hirayama, H., Nakagawa, S., Nunoura, T., Horikoshi, K., 2008. Cell proliferation at 122 °C and isotopically heavy CH4 production by hyperthermophilic methanogen under high-pressure cultivation. Proc. Natl. Acad. Sci. 105, 10949–10954..

Thomson, J., Wilson, T.R.S., Culkin, F., Hydes, D.J., 1984. Non-steady state diagenetic record in eastern equatorial Atlantic sediments. Earth Planet. Sci. Lett. 71, 23–30. https://doi.org/10.1016/0012-821X(84)90049-9.

Torres, M.E., Cox, T., Hong, W.-L., McManus, J., Sample, J.C., Destrigneville, C., Gan, H. M., Gan, H.Y., Moreau, J.W., 2015. Crustal fluid and ash alteration impacts on the biosphere of Shikoku Basin sediments. Nankai Trough, Japan. Geobiol. 13, 562–580. https://doi.org/10.1111/gbi.12146.

Tsang, M.-Y., Bowden, S.A., Wang, Z., Mohammed, A., Tonai, S., Muirhead, D., Yang, K., Yamamoto, Y., Kamiya, N., Okutsu, N., Hirose, T., Kars, M., Schubotz, F., Ijiri, A., Yamada, Y., Kubo, Y., Morono, Y., Inagaki, F., Heuer, V.B., Hinrichs, K.-U., 2020. Hot fluids, burial metamorphism and thermal histories in the underthrust sediments at IODP site C0023. Nankai Accretionary Complex. Mar. Pet. Geol. 112, 104080. https://doi.org/10.1016/j.marpetgeo.2019.104080.

Tsang, M.-Y., Wortmann, U.G., 2022. Sulfur isotope fractionation derived from reaction-transport modeling in the Eastern Equatorial Pacific. J. Geol. Soc. 179, 1–9. https://doi.org/10.1144/jgs2021-068.

Underwood, M.B., Guo, J., 2018. Clay-mineral assemblages across the Nankai-Shikoku subduction system, offshore Japan: a synthesis of results from the NanTroSEIZE project. Geosphere 14, 2009–2043. https://doi.org/10.1130/GES01626.1.

Volz, J.B., Liu, B., Köster, M., Henkel, S., Koschinsky, A., Kasten, S., 2020. Post-depositional manganese mobilization during the last glacial period in sediments of the eastern Clarion-Clipperton Zone, Pacific Ocean. Earth Planet. Sci. Lett. 532, 116012. https://doi.org/10.1016/j.epsl.2019.116012.

Wehrmann, L.M., Arndt, S., März, C., Ferdelman, T.G., Brunner, B., 2013. The evolution of early diagenetic signals in Bering Sea subseafloor sediments in response to varying organic carbon deposition over the last 4.3 Ma. Geochim. Cosmochim. Acta 109, 175–196. https://doi.org/10.1016/j.gca.2013.01.025.

Wellsbury, P., Goodman, K., Barth, T., Cragg, B.A., Barnes, S.P., Parkes, R.J., 1997. Deep marine biosphere fueled by increasing organic matter availability during burial and heating. Nature 388, 573–576. https://doi.org/10.1038/41544.

Wortmann, U.G., 2006. A 300 m long depth profile of metabolic activity of sulfate-reducing bacteria in the continental margin sediments of South Australia (ODP Site 1130) derived from inverse reaction-transport modeling. Geochm. Geophys. Geosyst. 7, Q05012. https://doi.org/10.1029/2005GC001143.

Yamano, M., Foucher, J.-P., Kinoshita, M., Fisher, A., Hyndman, R.D., 1992. Heat flow and fluid flow regime in the western Nankai accretionary prism. Earth Planet. Sci. Lett. 109, 451–462. https://doi.org/10.1016/0012-821X(92)90105-5.

Zeikus, J.G., Winfrey, M.R., 1976. Temperature limitation of methanogenesis in aquatic sediments. Appl. Environ. Microbiol. 31, 99–107. https://doi.org/10.1128/aem.31.1.99-107.1976.

Zindorf, M., März, C., Wagner, T., Gulick, S.P.S., Strauss, H., Benowitz, J., Jaeger, J., Schnetger, B., Childress, L., LeVay, L., van der Land, C., La Rosa, M., 2019. Deep sulfate-methane transition and sediment diagenesis in the Gulf of Alaska (IODP Site U1417). Mar. Geol. 417, 105986. https://doi.org/10.1016/j.margeo.2019.105986.